ICF Reactor Target Chamber Issues for the Los Alamos National Laboratory FIRST STEP Reactor Concept

Robert R. Peterson and Tim J. Bartel

June 1984

UWFDM-580

FUSION TECHNOLOGY INSTITUTE

UNIVERSITY OF WISCONSIN

MADISON WISCONSIN

ICF Reactor Target Chamber Issues for the Los Alamos National Laboratory FIRST STEP Reactor Concept

Robert R. Peterson and Tim J. Bartel

Fusion Technology Institute
University of Wisconsin
1500 Engineering Drive
Madison, WI 53706

http://fti.neep.wisc.edu

June 1984

UWFDM-580

ICF REACTOR TARGET CHAMBER ISSUES

FOR THE

LOS ALAMOS NATIONAL LABORATORY

FIRST STEP REACTOR CONCEPT

Robert R. Peterson and Tim J. Bartel

Fusion Engineering Program
Nuclear Engineering Department
University of Wisconsin
Madison, Wisconsin 53706

June 1984

UWFDM-580

I. Introduction

The FIRST STEP (Fusion, Inertial, Reduced-Requirements Systems Test for Special Nuclear Materials, Tritium, and Energy Production) is a concept for a facility that would simultaneously serve as a test bed for technology development and produce tritium, special nuclear materials and energy.[1] A schematic picture of the target explosion chamber and surrounding blanket structures is shown in Fig. 1. The target chamber consists of a spherical wall covered with a 1 to 5 cm thick layer of liquid metal, in the base case liquid lithium, which is flowing down the walls from an injection assembly at the top to an outlet duct at the bottom. There are two beam ports, for either heavy ion or laser beams, and target injection machinery at the top of the target chamber. The design is in an early stage and the subject of this report is the investigation into a few of the critical issues dealing with the target chamber and first wall.

The work reported here has examined four general issues: (1) bare first wall survival for high density cavities, (2) liquid metal vaporization and recondensation and the resultant maximum allowable repetition rate for micro-explosions, (3) stability of liquid metal layer under the influence of vaporization, and (4) leakage of target chamber material through the beam ports. The first item was done because there is the possibility that heavy ion beams can be propagated through 1 to 10 torr (0°C) of cavity gas[2] and if this is possible, the gas may sufficiently protect the wall from the target energy so that the liquid metal protection is not necessary. This is discussed in Section II. Items 2 through 4 are done under the assumption that a 1×10^{-3} torr target chamber gas is needed for beam propagation. Item 2 is very important to the design because of the high impact of the repetition rate on the

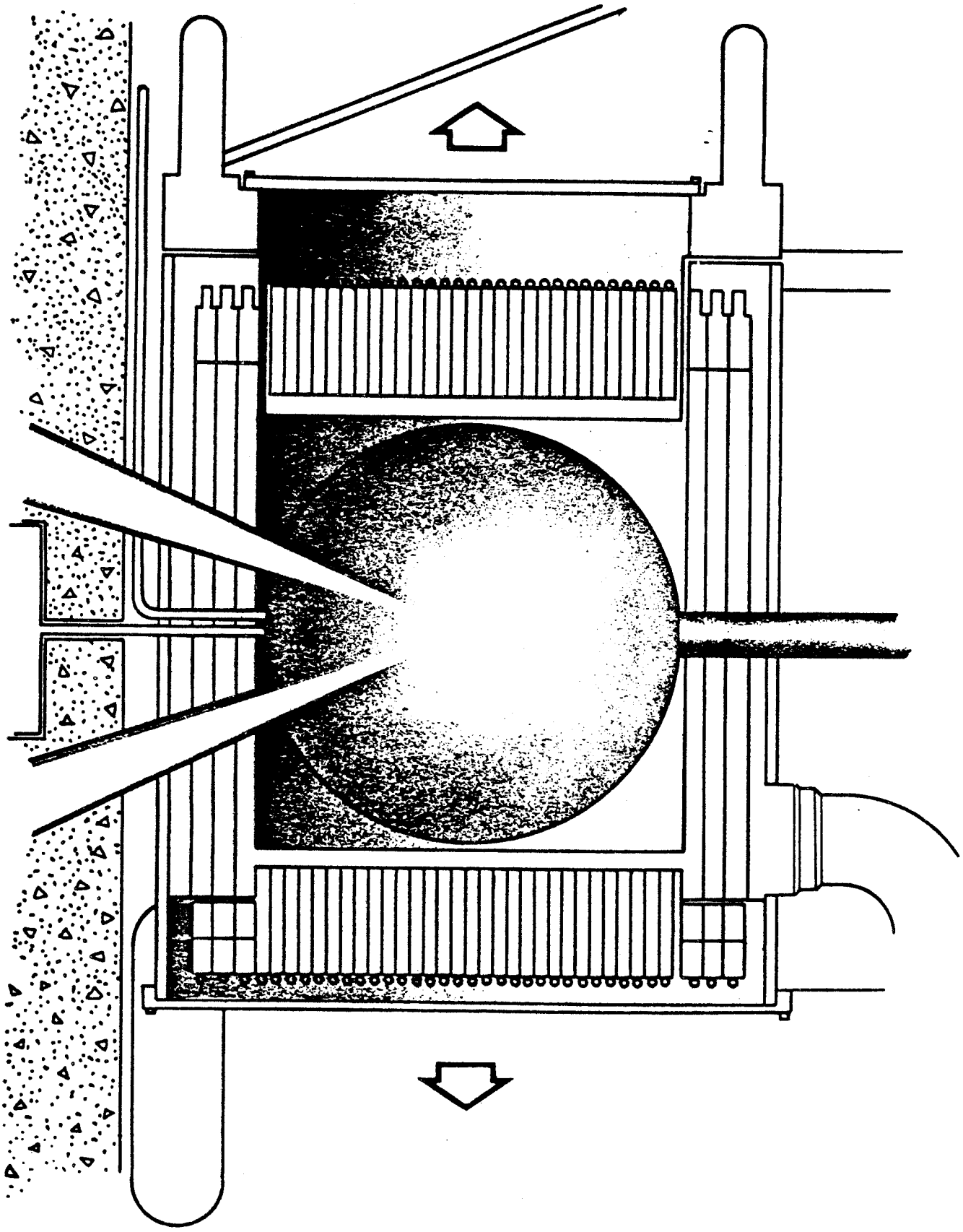

Fig. 1. Schematic Picture of the Target Explosion Chamber and Surrounding Blanket Structures for the FIRST STEP Design Concept.

economics of the plant. In order to do the calculations of vaporization and condensation of liquid metal, considerable computer code development had to be done. The code development is decribed in Section III, while the results pertaining to item 2 are presented in Section IV. Items 3 and 4 are discussed in Sections V and VI, respectively.

II. Bare Wall Cavities

The effects of the target explosion generated fireball in a 1 to 10 torr pure argon gas on an unprotected cavity first wall have been investigated. One option for propagation of a heavy ion beam to the target is in the so-called 1 torr window. There is the possibility that a background cavity gas at a density that would produce a 1 to 10 torr gas pressure at 0°C would repress the important plasma instabilities but would still allow the beam to propagate.[2] The results presented in this section will determine whether this cavity gas will absorb enough of the target micro-explosion x-ray and ion debris energy and transmit it to the first wall over a long enough time that a bare wall will survive. The target yield for these calculations is 25 MJ, the cavity radius is 2 meters and the gas is 1, 5 and 10 torr of pure argon.

The formation and propagation of the fireball in the cavity gas has been studied with the MFFIRE computer code.[3] This is a Lagrangian hydrodynamics and multifrequency radiation transfer code which uses equations-of-state and opacities provided by the MIXERG computer code. In all of these calculations, the x-ray spectrum from the HIBALL heavy ion beam target has been used,[4] where the spectrum has been scaled to give the proper amount of total energy in x-rays and debris ions. The HIBALL target is shown in Fig. 2 and the x-ray spectrum for a 25 MJ target micro-explosion is shown in Fig. 3. The ion

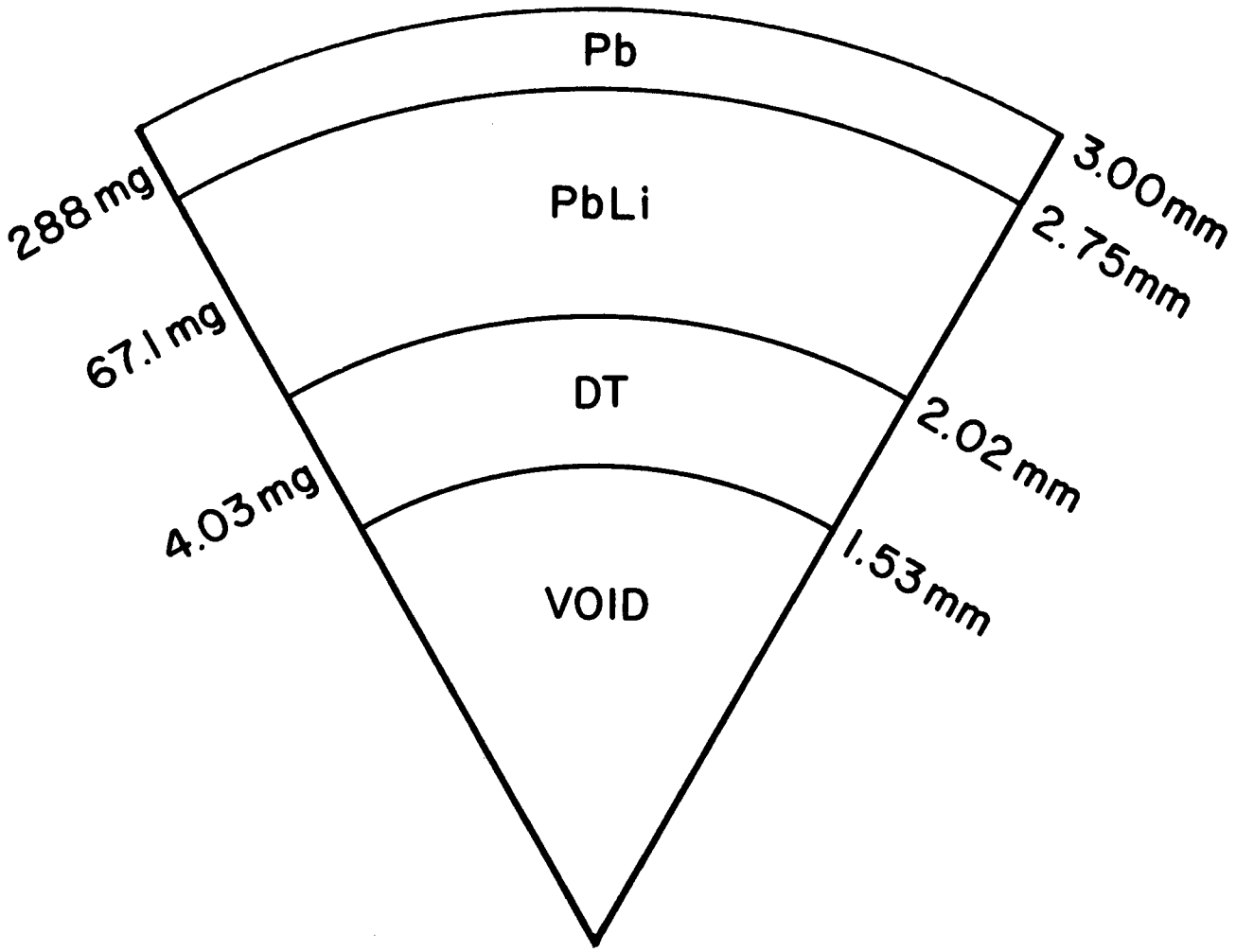

Fig. 2. The "HIBALL" Inertial Confinement Fusion Target.

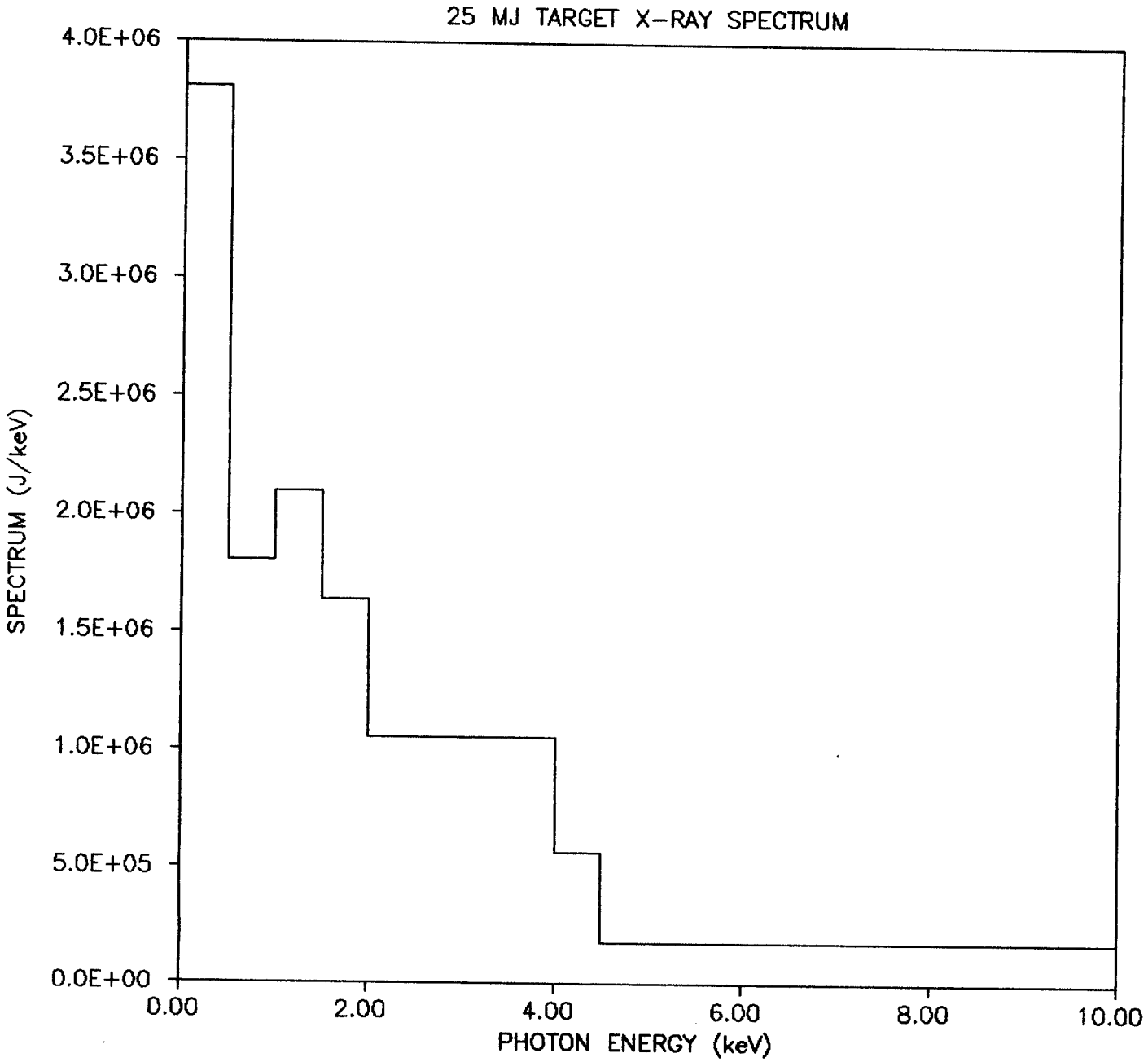

Fig. 3. X-ray Spectrum from a 25 MJ Microexplosion of a "HIBALL" Target.

debris energy has been added to the lowest energy group because the stopping of ions and of low energy x-rays in the gas occurs over similar lengths.

The results of these simulations are summarized in Table I. Four relevant quantities are presented for each of the three gas densities. The first of the quantities is the energy deposited in the gas by the x-rays and debris ions. These numbers should be compared with the total 7.5 MJ in x-rays and ions which emanate from a 25 MJ micro-explosion. One will note that, as the gas density increases, so does the fraction of the x-ray and ion energy which is absorbed in the gas. Next, one sees that the energy re-radiated to the wall by the gas is quite naturally tied to the energy initially absorbed by the gas. Since the fraction of the energy re-radiated to the wall within 1 ms of the target micro-explosion remains roughly constant, the total radiant energy increases with gas density. In a similar manner, the shock over-pressure that the fireball puts on the first wall increases with gas density. However, in this case there are two effects leading to this trend: first, the total energy stored in the gas grows larger at higher gas densities and second, the x-ray deposition profile is steeper and the shock stronger in dense gases. The final item tabulated is the radiant energy density on the first wall integrated over the first 1 ms after the target explosion. If there were no cavity gas, this number would be 14.9 J/cm over a very short time. This number and all of those in Table I are probably low enough that a metallic wall would not melt, but the radiant energy density is high enough in all cases that damage due to thermal stresses is a potential problem. The shock over-pressures are low enough that they will not cause severe design problems in themselves, but could work on the wall in the presence of large thermal stresses leading to accelerated crack growth and failure of the wall.

Table I. Fireballs in Pure Argon

Target Yield = 25 MJ; Radius = 2 m

Gas Density (torr 0°C)	1	5	10
Energy Deposited in Gas (MJ)	4.4	6.6	7.1
Energy Radiated to Wall in 1 ms (MJ)	2.9	4.0	4.3
Maximum Over-Pressure on Wall (MPa)	0.055	0.166	0.226
Energy Density Radiated to Wall in 1 ms (J/cm^2)	5.8	8.0	8.6

N.B. If there is no target chamber gas, the energy radiated to the wall is 7.5 MJ/shot and the energy density is 14.9 J/cm^2/shot.

The details of this process will naturally depend on the choice of first wall material and the design of the first wall.

In summary, unprotected walls in the FIRST STEP target chamber do not look promising either for cavity gases of 1 to 10 torr or for much less dense gases. The most obvious design change would be to increase the cavity radius but this would have a very negative impact on the rather large and complex blankets surrounding the target chamber. A second approach might be to line the inside of the wall with a material like silicon-carbide, which could withstand the high surface temperatures and re-radiate the energy to the first wall over a longer period thus reducing the thermal stresses in the wall itself.[5] A third method, and the one chosen in the study, is to coat the inside of the wall with a layer of liquid metal, in this case liquid lithium. The liquid metal will partially vaporize upon absorbing the x-ray and debris ion energy, converting most of the energy into heat of vaporization. The vapor will then condense back on the wall over a much longer time, a process which is the subject of much of the rest of this report.

III. Computer Code Development

A computer code, CONRAD, has been developed to simulate the vaporization, condensation and gas dynamics of liquid lithium vapor. This code has been created from the Lagrangian hydrodynamics code, MFFIRE, by adding a calculation of the temperature profile in the liquid metal film and the associated vaporization. As part of the conversion of this code, considerable effort has been put into a dynamic rezoning of the Lagrangian mesh and into interfacing the vaporization package with the cavity gas hydrodynamics. CONRAD is run in a manner very similar to the way MFFIRE is run, with only a few changes in the input. These additions to the input are discussed in this section and one

will be able to run CONRAD with the information presented here and by referring to the MFFIRE documentation.[3]

The surface vaporization package consists of a calculation of the time-dependent temperature profiles in the liquid metal layer and of the vaporization of liquid metal from the surface. The temperature profiles are calculated from radiant and condensation heat fluxes entering the liquid metal layer from the target chamber gas. The user has the choice of a fully implicit, fully explicit or something in between liquid metal temperature calculation; that choice is made by setting the parameter "theta" between 0 and 1, where 1 is fully implicit. The user also has the choice of Dirichlet, Neumann or Robbins boundary conditions at the front and back of the liquid metal by setting "11" and "1m", respectively, to 1, 2, 3. If the user wishes to use thermal properties which change throughout the calculation, the subroutine "FPROP" must be programmed to do so. The temperature profiles are calculated with a traditional tri-diagonal matrix solver. The heat flux into the liquid metal may be volumetric, where the heat flux is broken into up to 25 groups with each group having a linear attenuation coefficient, fxmu (1/m), and a surface volumetric heat flux, qint (MW/m^2). If the number of groups, nvol, is set to zero then a surface heat flux is assumed. The portion of the surface zone which is vaporized is determined by conservation of energy: the vaporized mass is just the energy absorbed by the zone on the current time step minus the sensible heat required to raise the zone up to its local boiling point, tbp (K), all divided by the local heat of vaporization. The local boiling point is, in the current version of the code, a constant defined for each zone at the start of the simulation. An interesting modification to CONRAD would be to calculate tbp in the subroutine "FPROP" as a function of

the pressure of the target chamber gas at the surface of the liquid metal. The main subroutine of the vaporization package is "FILM", which makes calls to "ONED" where the temperature profiles are calculated, to "ENDBC" where boundary conditions are set, to "FPROP", which has already been discussed, and through "ONED" to "TRIDIG", which is a tri-diagonal solver. Initialization of parameters used in the vaporization package is done in subroutine "INITF".

The surface heat flux and the exchange of mass between the target chamber gas and the liquid metal are calculated in CONRAD's interface subroutine, "WXCHNG". The surface heat flux is the sum of the condensation heat flux, the condensation rate times the sum of the specific energy density of the vapor and the heat of vaporization, plus the radiation heat flux, consisting of unattenuated target x-rays and thermal radiation emitted by the gas. The radiant portion of the heat flux may be broken into up to 25 energy groups. In calculating the condensation rate, it is assumed that 25% of the vapor atoms within a mean-free-path of the surface are moving towards the surface and that all of the atoms reaching the surface will stick. Mass that is exchanged between the surface and the gas is uniformly deposited in or lost from the Knudsen boundary layer,[6] where the width of this boundary layer is recalculated on each time step. In this subroutine, care has been taken to assure that energy is conserved in the exchange of mass.

Since CONRAD uses a Lagrangian differencing scheme for both hydrodynamics and heat transfer, the variable total gas mass brought about by condensation and vaporization has required the implementation of dynamic rezoning of the one-dimensional mesh. The rezoning is initiated and controlled by the subroutine "REZONE", which calls the subroutine "ZONER". CONRAD calls "REZONE" if the fractional mass change of any zone is more zoning. The parameter

"rzcm" is set during the initialization phase of the simulation. If isw(17) is negative, rezoning is not done under any circumstances. In rezoning, the ratios of the masses of the zones are kept at the initial values. As the zoning is shifted all variables such as density and temperature are recalculated in the new mesh by interpolation.

There are only a few differences between the running of CONRAD and MFFIRE, and most of them are just the additional input parameters listed in Table II. Some of these have already been discussed and many of the rest are self-evident from the comments in the table. In Table II, the types of the variables are given as either real vectors (RV), real scalars (RS), integer vectors (IV), or integer scalars (IS). There have also been some additions to the switching vector, isw(50). If isw(17) is non-positive, there is no rezoning. The default for isw(17) is 0. If isw(20) = 0, the default value, CONRAD does no vaporization or condensation and runs very much like MFFIRE, while isw(20) = 1 switches on the vaporization package. Another difference between CONRAD and the version of MFFIRE described in the documentation is that the latter is written to run on the UNIVAC 1100 at the University of Wisconsin, where double-precision variables are required, while CONRAD runs on a CRAY-I at Los Alamos National Laboratory, where the single-precision words have roughly the same accuracy as double-precision on the UNIVAC. Sample input is shown in Table III for the run which yields the results discussed in Section IV. Notice that all of the real variables input are single-precision.

Table II. Additional Input Variables for CONRAD

Variable	Type	Default Value	Description
rzcm	RS	0.01	allowed fractional mass change for zones between rezonings
nx	IS	---	initial # of zones in film
delx(100)	RV	---	initial zone widths in film (m)
rhoflm(100)	RV	---	density of film (kg/m^3)
tbp(100)	RV	---	local boiling point (K)
xk(100)	RV	---	local thermal conductivity (MW/m-K)
rhohfg(100)	RV	---	local heat of vaporization (MJ/m^3)
mat(100)	IV	---	material type # for each zone
cp(100)	RV	---	local specific heat (MJ/kg/K)
t(100)	RV	---	initial local film temperatures (K)
cmfilm	RS	0.	total mass condensed over simulation (gm)
theta	RS	---	degree of implicitness (0. to 1.)
bc1	RS	---	wall temperature (K)
l1bc	IS	---	boundary condition index on outside of film (zone #1) (Dirichlet = 1, Neumann = 2, Robbins = 3)
eps	RS	1.	surface emissivity of film and last zone of gas
conv	RS	0.05	convergence accuracy in iteration on vaporization rate
awfilm	RS	---	atomic weight of film (amu)
z2b(53)	RV	---	local ionization level of gas (e)
qint(25)	RV	---	surface volumetric heat flux (MW/m^2)
fxmu(25)	RV	---	linear attenuation coefficient (1/m)
nvol	IS	---	# of volumetric heating groups

Table III. Sample CONRAD Input File

```
$input
   jmax=50
   nmax=5000,
   tmax=1.,
   dn2b=50*8.17e17,
   r1b=0.,20.,40.,60.,70.,80.,
   81.,82.,83.,84.,85.,
   86.,87.,88.,89.,90.,
   91.,92.,93.,94.,95.,
   96.,97.,98.,99.,100.,
   101.,102.,103.,104.,105.,
   106.,107.,108.,109.,110.,
   112.,114.,116.,118.,120.,
   122.,124.,126.,128.,130.,
   132.,134.,136.,138.,200.,
   tn2c=50*0.1379,
   tr2c=50*0.1379,
   atw2b=50*7.,
   nfg=20,
   radius=200.,
   ro=195.5,
   no=5,
   ri=10.,
   pmass=0.,
   ni=3,
   flux=8.1e6,
   jk=20,
   iz=3,
   xehist=0.e0,.5e0,1.e0,1.5e0,2.e0,2.5e0,3.e0,3.5e0,4.e0,4.5e0,5.e0,
          5.5e0,6.e0,6.5e0,7.e0,7.5e0,8.e0,8.5e0,9.e0,9.5e0,10.e0,
   xamp=3.816e6,1.806e6,2.1e6,1.638e6,4*1.056e6,0.564e6,11*0.1764e6,
   nx=20,
   delx=15*.0001,2*5.e-5,2*1.e-5,5.e-6,
   theta=1.,
   mat=20*1,
   eps=0.9,
   xk=20*7.1e-5,
   rhoflm=20*5.3e2,
   tbp=20*1000.,
   awfilm=7.,
   cp=20*3.57e-4,
   rhohfg=20*1.07e4,
   llbc=1,
   bcl=773.,
   t=19*773.,1000.,
   isw(1)=0,
   isw(4)=1,
   isw(5)=15,
   isw(11)=1,
```

```
isw(17)=1000,
isw(20)=1,
con(21)=0.,
iobin=15,
iedit(91)=100,
iedit(92)=1,
io=3*100 $
```

IV. Liquid Metal Vaporization and Condensation and the Target Chamber Rep Rate

The vaporization and condensation hydrodynamics code, CONRAD, has been used to simulate the vaporization of liquid metal off of the walls of the FIRST STEP target chamber and the subsequent condensation of the vapor back onto the walls. These phenomena are depicted schematically in Fig. 4. The simulations are broken down into 2 parts: first, the vaporization of large amounts of liquid metal by the target energy is calculated and then the condensation back onto the walls. The problem is split in this way to avoid certain numerical difficulties which can arise from trying to handle both parts in the same simulation. The first calculation provides the total vaporized mass and the total energy in that vapor. The mass is then spread out in some profile determined analytically by the user, the temperature is determined to put the correct amount of energy into the vapor and the second half of the calculation is started. It should be possible to do the whole simulation in one run by making sure that the equation-of-state data tables span the whole range of densities (perhaps 8 orders of magnitude) and by carefully controlling the rezoning process. This was not done for this calculation in the interest of obtaining an earlier result, since the optimization of the rezoning could be rather time consuming. The only relevant error in splitting up the problem occurred because the time that it takes the vapor to reach the state where the second simulation is started is not taken into account. However, it is straightforward to obtain an estimate of this time lag.

The vaporization phase of this calculation uses the spectrum of target x-rays shown in Fig. 3, scaled to the proper total energy. The width of the x-ray pulse is equal to isw(2) times the initial time step. The total target

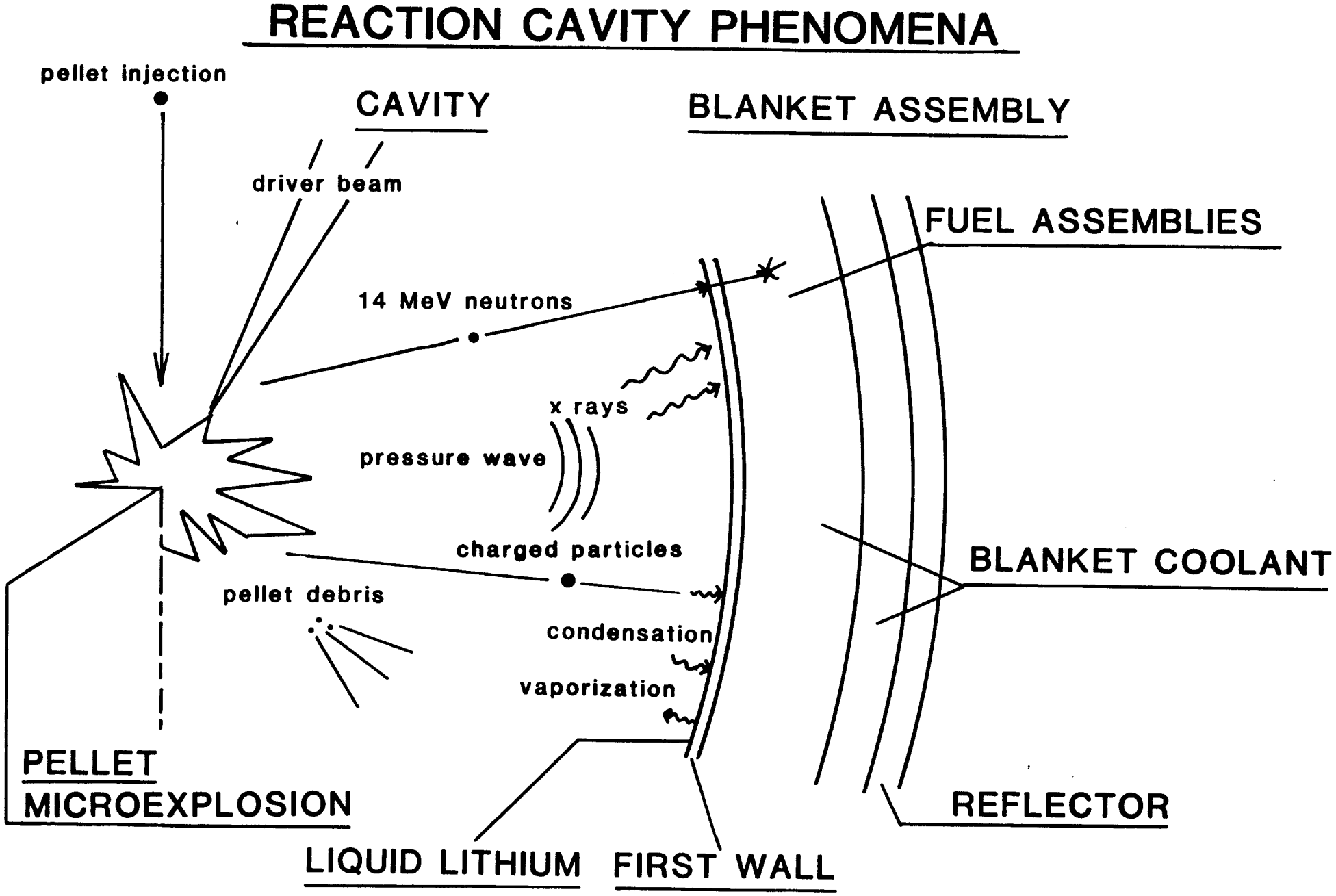

Fig. 4. Target Chamber Phenomena in the FIRST STEP.

yield was varied between 15 and 60 MJ. The target chamber parameters are listed in Table IV. The most relevant of the parameters are the 2 meter radius for the spherical chamber and the liquid metal material choice of liquid lithium. These parameters represent a base case for the purpose of obtaining numerical results and in no way should it be implied that a point design has been chosen. The amount of vaporized mass is plotted against target yield for the base case in Fig. 5. This is essentially linear in target yield because the time over which the target energy is deposited is very short compared to the temperature diffusion time scale; the x-ray pulse is only on the order of a nanosecond wide. The base case target yield is 23 MJ so that the vaporized mass is 318 g. The vapor used in the condensation phase of the calculation thus begins with this amount of mass at a temperature of 1000 K.

The condensation phase is simulated with CONRAD, using the input in Table III. One thing to notice in this input data is that con(21) is set to zero. This turns off the artificial viscosity term in the hydrodynamics: the artificial viscosity has dubious meaning in a non-shock situation and adds an unphysical work term to a condensation problem. The initial state for this simulation is taken as a uniform gas at a temperature of 1000 K and a density of 8.17×10^{17} particles/cm^3, which corresponds to a gas mass of 318 g. The film temperature profile is taken to be the same as at the end of the vaporization run. One expects a decompression wave to propagate into the gas as gas is lost from the cavity due to condensation, and in fact this is what one sees when the mass density is plotted against position and time as it is in Fig. 6. The decompression in the center of the cavity is not understood at this time but the amount of mass in these zones is small and there is probably not a large effect on the general results. The gas temperature is found to drop

Table IV. FIRST STEP Target Chamber Parameters

Target Chamber Design	Spherical
Target Chamber Radius	2 meters
# of Beam Ports	2
Radius of Beam Ports	20 cm
# of Coolant Ports	2
Radius of Coolant Ports	5 cm (upper) 20 cm (lower)
Nominal Target Yield	23 MJ
Target X-Ray Spectrum	"HIBALL"
First Wall Protection	Liquid Lithium
Liquid Lithium Thickness	1 cm
First Wall Temperature	500°C
Vapor Density Required for Heavy Ion Beam Propagation	4×10^{13} cm
Desired Repetition Rate	10 Hz

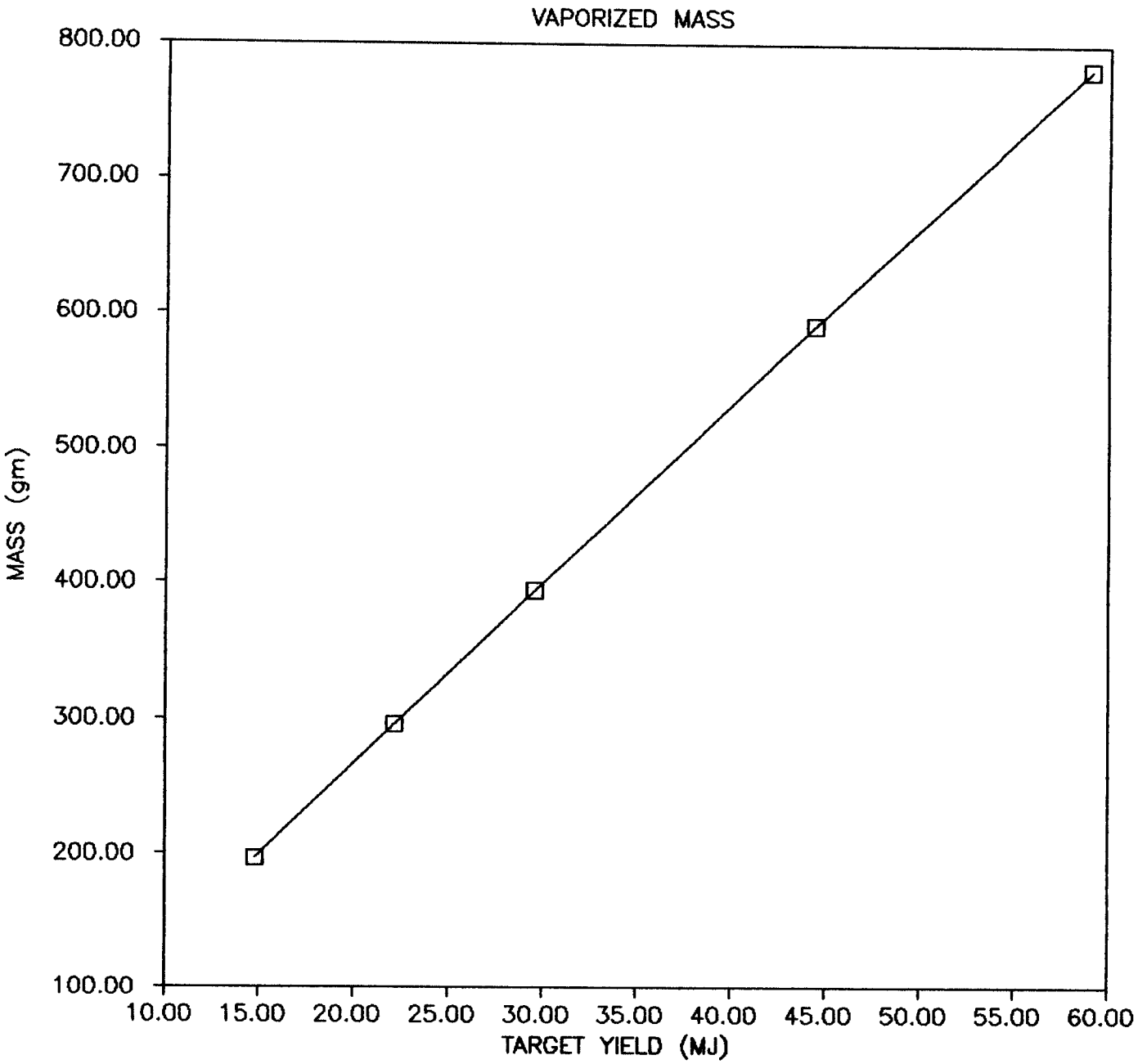

Fig. 5. Total Vaporized Mass Versus Target Yield for the FIRST STEP Base Case Design.

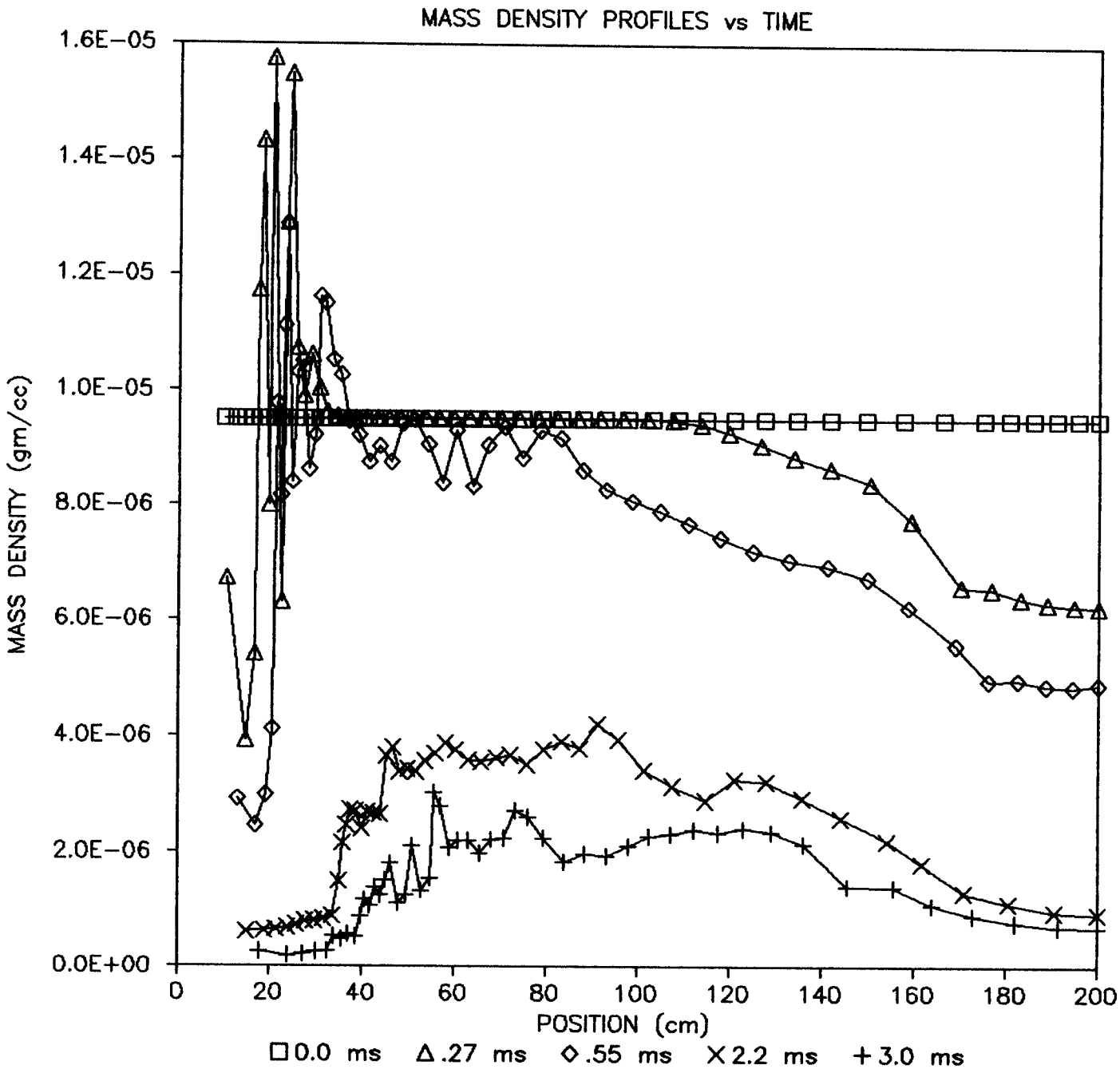

Fig. 6. Mass Density of Vapor in the Target Chamber Versus Position for Various Times After the Start of the Condensation Phase.

somewhat due to decompression and this has the effect of slowing the condensation a little from what one would expect from a constant temperature approximation.

The details of the condensation process affect the performance of the target chamber in determining the gas clearing time. The gas mass in the cavity and the log of the average number density are plotted against time in Fig. 7 and Fig. 8, respectively, for the base case design and the nominal target yield of 23 MJ. The calculation automatically stops when the size of the condensation Knudsen boundary becomes as large as the size of the cavity. This occurs at a density of 6.5×10^{23} cm^{-3}, 25 ms after the start of the simulation. As soon as the whole gas is within the boundary layer, the density should rapidly fall to 4×10^{13}. One should notice that the average density almost follows an exponential decay law.

From these results one can estimate the cavity gas clearing time and thus the allowable repetition rate. The velocity of sound in the vapor shortly after vaporization is 1.2×10^4 cm/s and so the vapor should take 16 ms to reach the initial state for the condensation phase of the simulation. The total elapsed time after the shot for the gas to reach the density required for beam propagation is thus 41 ms. A repetition rate of 20 Hz seems entirely possible and a design requiring 10 Hz is conservative.

V. Rayleigh-Taylor Stability of Liquid Metal Layer During Vaporization

The vaporization of the liquid metal by the target generated x-rays imposes a recoil force on the unvaporized liquid which may drive the layer Rayleigh-Taylor unstable. There may in fact be situations, as at the top of the cavity where the recoil force is opposed by the force of gravity, where the effect of the micro-explosion is to make the layer more stable. In this

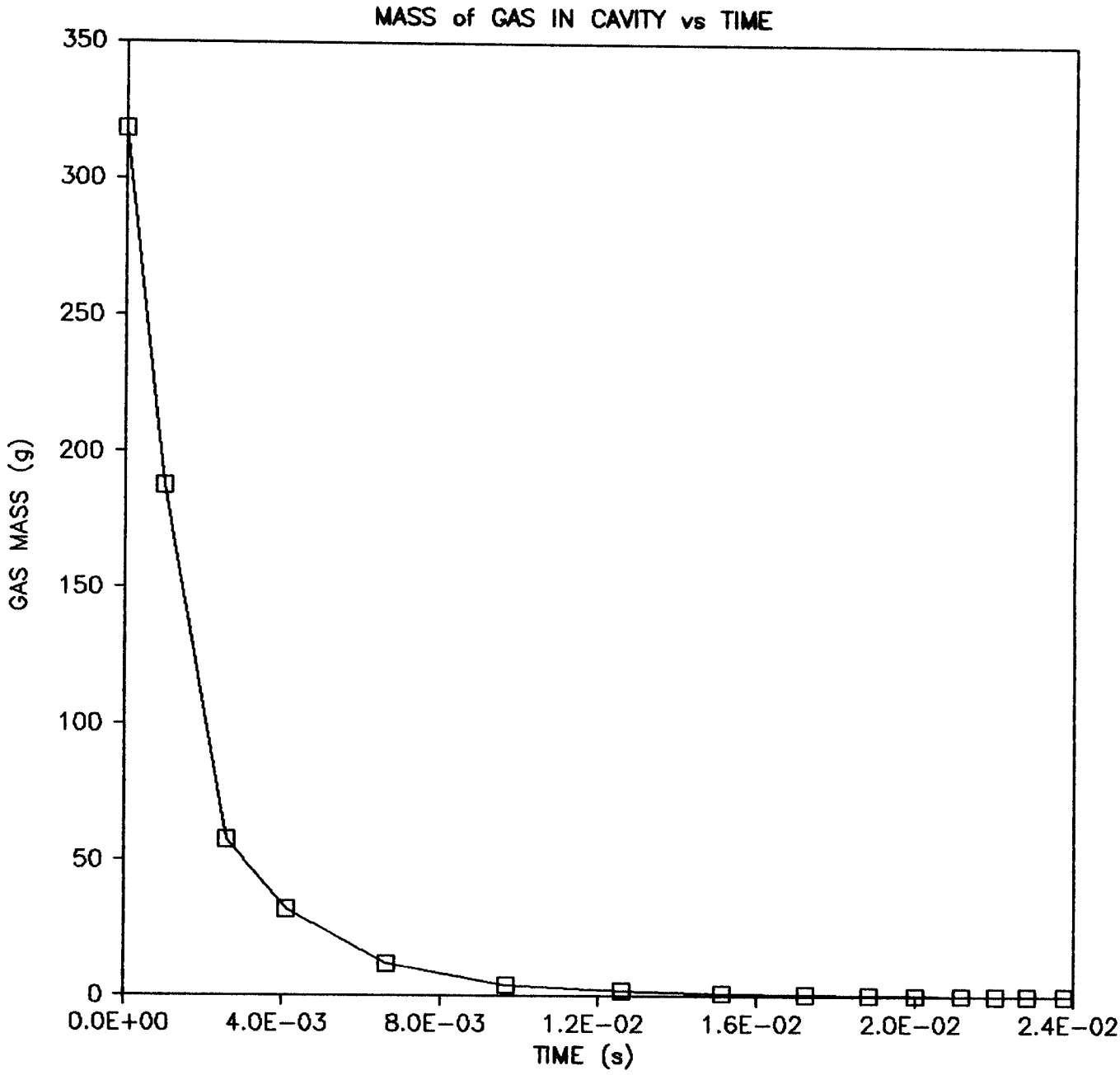

Fig. 7. Total Mass of Vapor in the FIRST STEP Target Chamber Versus Time After the Start on the Condensation Phase.

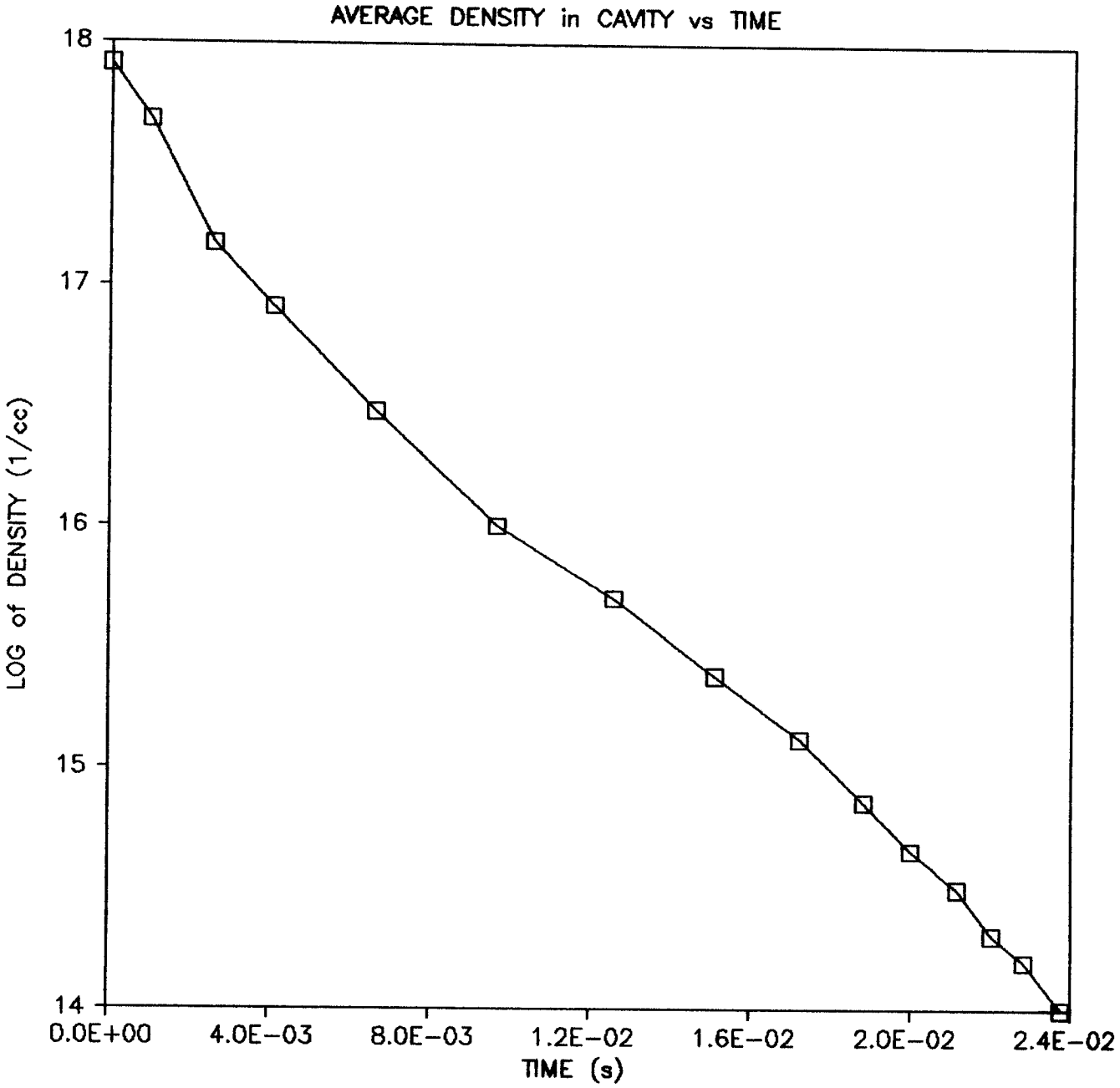

Fig. 8. Log_{10} of the Average Number Density in the Target Chamber of the FIRST STEP Versus the Time After the Start of the Condensation Phase.

work the recoil force is assumed to be oriented so that the layer is driven unstable. The growth rate of the instability is calculated and multiplied by the length of time that the recoil impulse is felt by the liquid metal to determine the amplitude of the most unstable mode at the end of vaporization.

The growth rate of the Rayleigh-Taylor instability is calculated with the method of Feldman.[7] This approach assumes that the viscosity of the liquid metal is uniform. Temperature dependence of the viscosity can lead to a viscosity profile across the liquid metal which may change the growth rate but this effect is ignored in this work. The method makes use of a dispersion relation for disturbances on the surface of the liquid.[18] The coefficients in this relation are formulated as functions of a surface Weber number,

$$W = fh^2/\sigma \ , \tag{1}$$

and a surface Reynolds number,

$$R = (f\rho_\ell)^{1/2}h^{3/2}/\eta \ , \tag{2}$$

where h is the thickness of the film, f is the recoil force per unit area, σ is the surface energy per unit area and η is the viscosity. The mass density of the liquid is ρ_ℓ. The recoil impulse for the base case design with a 23 MJ target yield is 120 dyne-s/cm^2, which allows f to be expressed in terms of the duration of the impulse, Δt. At a liquid temperature of 500°C, σ = 343.2 erg/cm^2 and $\eta = 0.34 \times 10^{-2}$ dyne-s/cm^2. When these values are inserted into Eqs. (1) and (2), one obtains,

$$W = 3.41 \times 10^{-1} \, h^2/\Delta t \tag{3}$$

and,

$$R = 2.31 \times 10^{3} \, h^{3/2}/(\Delta t)^{1/2} \tag{4}$$

where h is the thickness of the liquid metal in cm and Δt is the duration of the recoil impulse in seconds.

Using the dispersion relation and the fluid parameters R and W defined in terms of system quantities, the stability constraints can be found. The wavenumber at which the surface disturbance is growing most rapidly is found from the dispersion relation and this critical wavenumber times the thickness of the layer, h, is plotted against W and R in Fig. 9. The growth rate of this most unstable disturbance in s^{-1} is shown in Fig. 10, plotted against R and W. The dashed lines in Fig. 10 are for an exponential viscosity profile, where one can see the increase in growth rate for non-uniform viscosity. An example stability analysis, summarized in Table V, has been done for $\Delta t = 10^{-5}$ s and h = 1 cm and 5 cm, values that are somewhat arbitrary. One can see that, for both cases, the growth integrated over the duration of the recoil impulse is very small.

VI. Leakage of Liquid Metal into Beam Ports

One concern in a liquid metal first wall protection scheme is that vaporized material will leak out of the target chamber through holes provided for beam propagation. This vapor could cause pumping problems if a high vacuum is required in the final beam optics, as in the case of heavy ion beams, or could foul the optics of a laser driver. Additionally, there is the different but related problem of non-condensible gases consisting of fusion products and un-

Table V. Stability of Liquid Metal Layer

Layer Thickness (cm)	R	W	Growth Rate (s^{-1})	Growth Rate x Δt
1	7.3×10^5	3.4×10^4	< 10	$< 10^{-4}$
5	8.2×10^6	8.5×10^5	< 100	$< 10^{-3}$

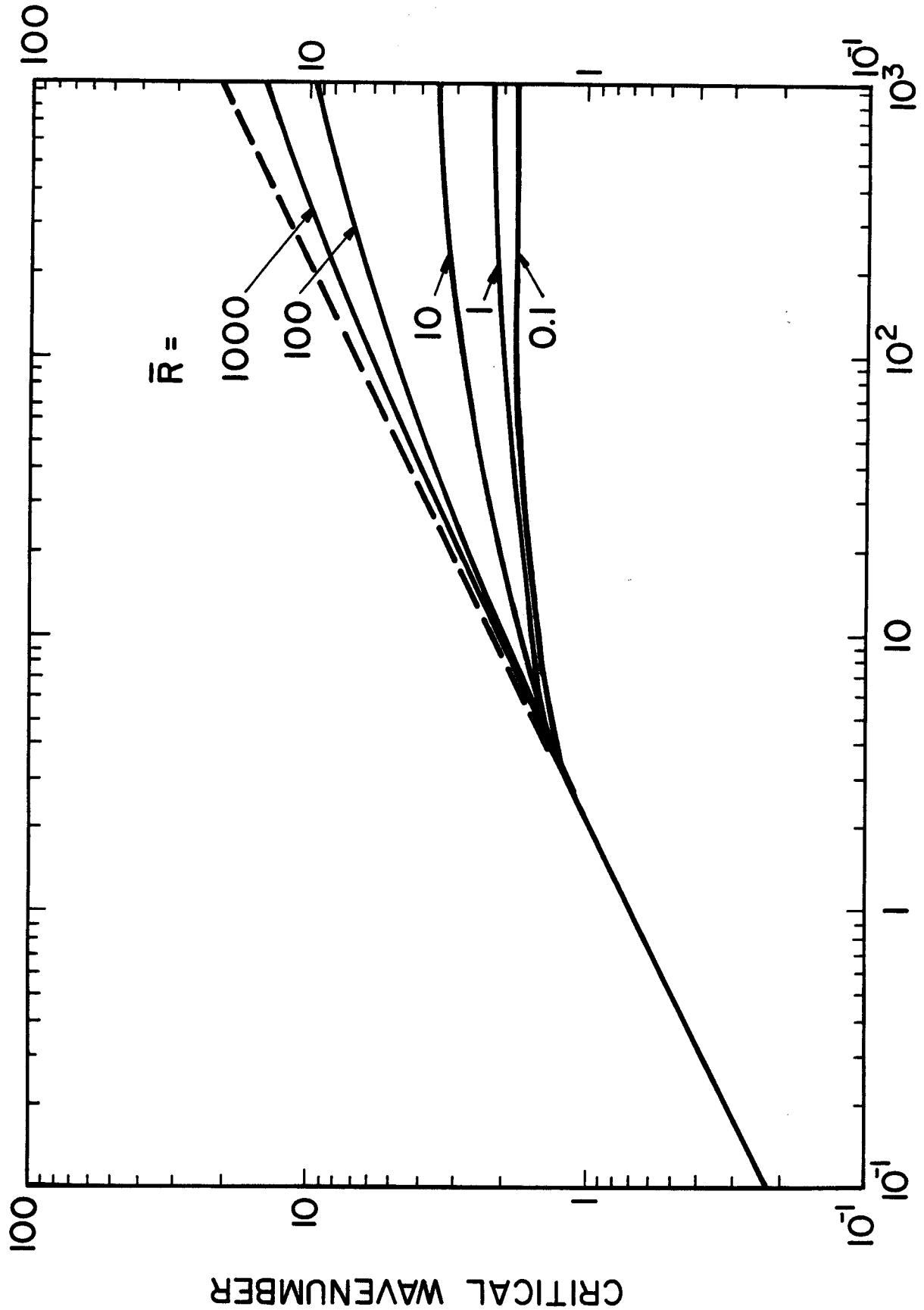

Fig. 9. The Rayleigh-Taylor Critical Wave Number Times the Liquid Layer Thickness Versus the Surface Reynolds and Weber Numbers.

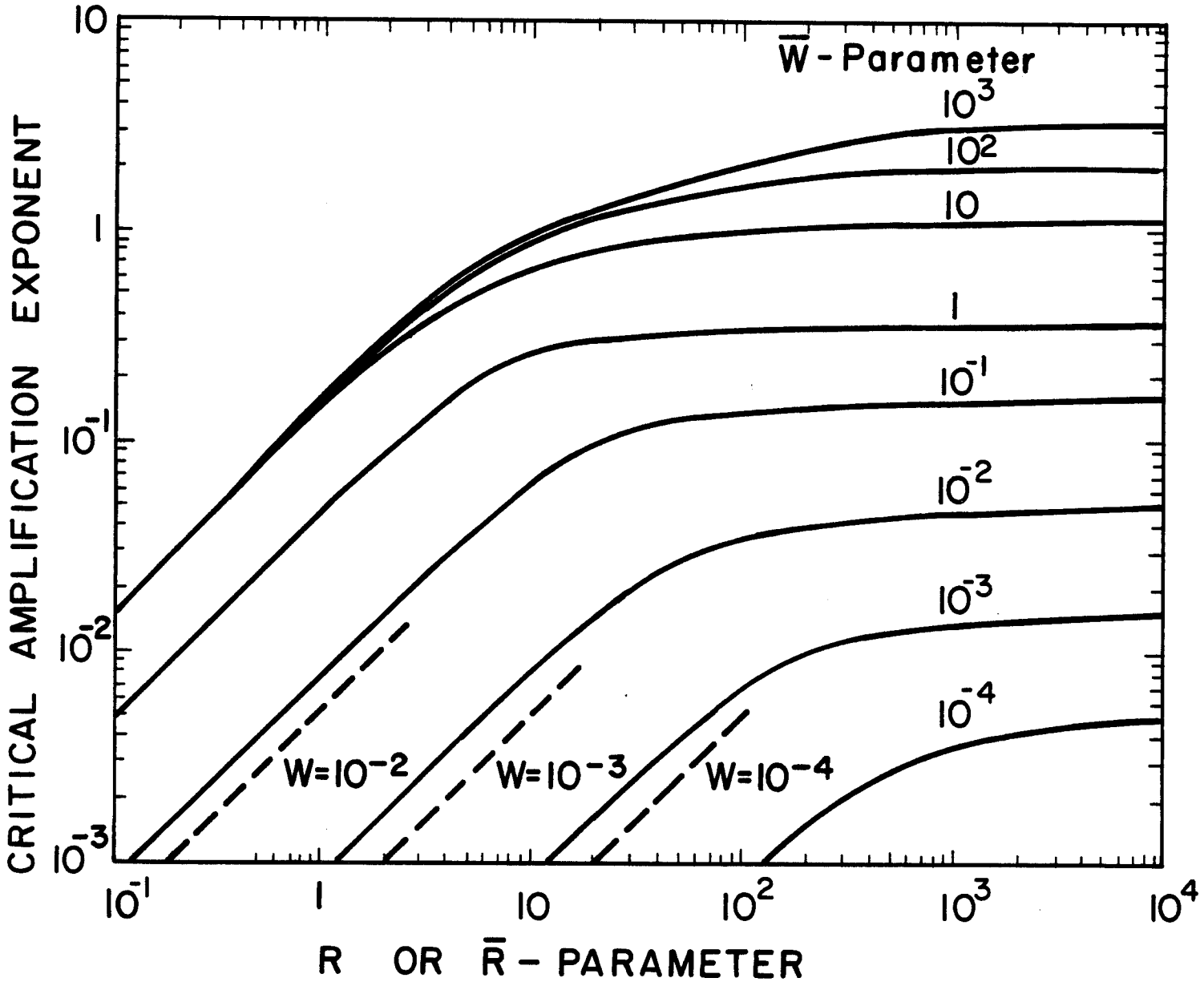

Fig. 10. The Rayleigh-Taylor Growth Rate at the Critical Wave Number Versus the Surface Reynolds and Weber Numbers.

burned fusion fuel that can build up in the target chamber and flow into the beam ports.

The problem posed by the vaporized liquid metal is handled by cooling the beam port so that the liquid metal vapor condenses. The beam ports are situated above the target chamber so that the condensed liquid metal will just run out of the beam port into the cavity. For the FIRST STEP base case parameters and a 23 MJ target yield, only 0.5% of the wall area is taken by beam ports so that just 1.6 gm of liquid lithium enters the beam ports per shot. Dripping will not be a problem because the geometry of the beam ports and the target chamber precludes interference by a drop with the beam propagation or target injection. In the heavy ion beam case, one can assure that very little vapor will reach the end of the beam port nearest the accelerator by curving the port and the path of the beam ions with magnetic fields. In the case of lasers, one cannot curve the beam port between the final optics and the target chamber but one can use a gas to sweep any vapor away from the optical surfaces. In either case, the amount of vaporized material in the beam port is small and there are solutions to the problem.

The removal of non-condensible gases consisting of unburned fuel and helium ash must be accomplished through some active means.[9] The hydrogen isotopes in the fuel will probably be absorbed in the lithium and they will not be considered here. Some of the helium will be absorbed in the lithium, but for what follows it will be assumed that active pumping is the only way to remove the helium. The helium pumping parameters are given in Table VI. These values are for the base case with a 23 MJ target explosion. The pressures are all calculated assuming that helium is an ideal gas. The required throughput is just the chamber volume times the gas pressure increase

Table VI. Helium Removal Parameters

Target Chamber Volume (cm^3)	3.35×10^7
Repetition Rate (Hz)	10
Total # of Helium Atoms Created per Shot	8.05×10^{18}
Number Density Increase per Shot (cm^{-3})	2.4×10^{11}
Gas Temperature (K)	1000
Gas Pressure Change per Shot (torr)	2.52×10^{-5}
Required Number Density (cm^{-3})	1×10^{13}
Required Pressure (torr)	1.05×10^{-3}
Required Throughput (torr-ℓ/s)	8.43
Required Pumping Speed (ℓ/s)	8.04×10^3
Duty Factor (%)	85
Cryopanel Area (m^2)	0.473
Pumpdown Time (s)	0.1

per shot times the repetition rate. The required pumping speed is the ratio of the throughput and the required pressure. The duty factor refers to the fraction of time that each cryopanel is available for pumping. The remainder of the time the cryopanel must be regenerated. Assuming that cryopumps can pump helium at 2 ℓ/s for every cm^2 of adsorbing area, the duty factor and the required pumping speed lead to a required surface area of 0.473 m^2. This value is based on the assumption that the resistance to the pumping by the beam port is negligible. The time that it takes the gas pressure to get back to the required value can be expressed as

$$t = V/S \ln (p_1/p_2) , \quad (5)$$

where V is the target chamber volume, S is the pumping speed, p_1 is the gas pressure shortly after the target explosion and p_2 is the required gas pressure. The parameters in Table VI lead to a recovery time of 0.1 s, just barely adequate for a 10 Hz repetition rate. This shows that a more careful consideration of the helium pumping and a design of a system with a higher pumping speed are needed.

VII. Conclusions

Some issues critical to the design of the FIRST STEP target chamber and first wall have been examined. These have included vaporization and recondensation of liquid metal, the effect of these on the target chamber repetition rate, the effect of rapid vaporization on the Rayleigh-Taylor stability of the liquid metal layer, and the leakage of target chamber materials out of the beam ports. There has been nothing associated with any of these issues which would deny the feasibility of the FIRST STEP with the base case parameters.

The repetition rate allowed by liquid metal recondensation is greater than 10 Hz. The growth rate for the Rayleigh-Taylor instability in the liquid metal is low enough that the most unstable disturbance does not have time to grow much during the recoil due to vaporization. Liquid metal vapor from the target chamber can easily be condensed on the walls of the beam ports so that very little of it will reach the front end of the driver. Non-condensible gas buildup can be handled by adsorbing the hydrogen isotopes in the liquid lithium and by cryopumping the helium out the beam ports, though a more complete design and analysis of the latter is needed.

In order to do the calculations concerning vaporization and condensation, a large amount of computer code development was required. The resulting code, CONRAD, uses a dynamic rezoning of the Lagrangian mesh to properly simulate the behavior of a gas which is gaining or losing mass. The necessary information for running CONRAD is included in this report and in the MFFIRE documentation. Before stand-alone documentation will be written for CONRAD, additional development and testing of the code should be completed.

There are many target chamber issues which have not yet been addressed for the FIRST STEP. Among these are the heating and coating of the target by the liquid metal vapor during target injection and other stability issues dealing with the liquid metal layer. Also, a base case design of the non-condensible gas pumping system and a consideration of the effects of the finite conductance of the beam ports on the pumping are needed. Finally, the design of the FIRST STEP is evolving and the calculations presented in this report should be repeated in an attempt to optimize the target chamber design.

Acknowledgement

This work was supported by the Department of Energy, Office of Inertial Fusion, under contract no. DE-AS08-83DP40183.